Feynman path description of the effects of dephasing of spatial coherences on the transmission and reflection probabilities through a one-dimensional potential

Karna Nagalla and Jamie D. Walls*

Department of Chemistry, University of Miami, Coral Gables, Florida 33146,USA

(Dated: December 14, 2022)

Abstract

In this work, we examine the effects of spatial dephasing of coherences on the transmission and reflection probabilities for electrons with energy E incident to a one-dimensional rectangular barrier of height V_0 . Statistical models are presented where the coherence between different scattering pathways or "Feynman paths" undergo dephasing over a length scale, L_{ϕ} . For incident waves with $E > V_0$, three different dephasing models that attenuate the contributions of spatial coherence to the transmission and reflection probabilities while preserving unitarity (i.e., conserving charge) were investigated. In the tunneling regime (incident waves with $E < V_0$), however, preserving unitarity requires $L_{\phi} \to \infty$, suggesting that elastic tunneling through a rectangular barrier is 100% spatially coherent for these dephasing models. However, wave absorption models are shown to preserve unitarity in the tunneling regime, which is not the case for scattering above the barrier.

^{*} Corresponding author: jwalls@miami.edu

I. INTRODUCTION

An important characteristic of mesoscopic and nanoscale electronic devices is the presence of phase-coherent electron transport due to the intrinsic wave-particle duality that charge carriers possess. As a result of phase-coherence, a variety of quantum mechanical interference phenomena can be observed in such devices, such as the Aharonov-Bohm effect[1], Anderson[2] and weak[3] localization, and modulations of the local density of states for quantum corrals formed on noble metal surfaces [4, 5] just to name a few. Such spatial interference is observed when a quantum particle's wave function can be represented by a coherent superposition of different trajectories or pathways between two points in space, as illustrated in Fig. 1(A). As long as the coherence between different pathways is preserved, i.e., there is no "which way" information provided either through direct measurement by an observer or due to interactions with the environment [6, 7], interference between pathways can be observed. Transport can be considered phase-coherent or within the phase-coherent regime over a length scale defined by the phase coherence length, L_{ϕ} . Generally, coherence between different pathways decays exponentially with the difference in path length relative to L_{ϕ} . If spatial coherences are completely dephased, then pathways between two points in space no longer add coherently as illustrated in Fig. 1(B). This loss of coherence and/or dephasing will also weaken many of the interference phenomenon listed above.

A variety of models have been proposed to describe dephasing in mesoscopic systems. One of the earliest and still most widely used phenomenological method for modeling dephasing in electron transport was proposed by Buttiker[8] in which a fictitious dephasing probe/reservoir is connected to the device[8]. In this model, electrons are effectively absorbed and then reinjected with a random phase back into the device, resulting in dephasing. While the dephasing probe model is consistent with microscopic pictures of decoherence[9–11], the dephasing is localized to the region of the dephasing probe in the device. Modifications to Buttiker's model have included multiple dephasing probes so that dephasing occurs throughout the device[12]. It should be noted that dephasing probes do not simply result in "pure" dephasing but also cause some momentum randomization for the reinjected electrons, and recent theoretical models[13] of dephasing have been proposed where the relative amounts of momentum and phase randomization can be controlled.

Alternative models of for modeling dephasing in electron transport have also been pre-

sented. These methods mostly rely on a scattering "pathway" picture in which dephasing of spatial coherence can be understood by viewing transport in terms of multiple, one-dimensional bouncing pathways or Feynman paths[14] that the electrons follow before ultimately being transmitted, analogous to optical Fabry-Perot resonances that occur between two interfaces[15, 16]. These models have mainly been used to describe dephasing in Aharonov-Bohm experiments[17] or for resonant tunneling of electrons in double barrier structures[18–23]. In wave or stochastic absorption models[24], the wave function is exponentially attenuated with each successive bounce within the device. While analogous models have been used in Fabry-Perot etalons to describe the change in photon numbers due to absorption[25], the number of electrons is conserved in a closed system, and these absorption models therefore do not conserve electron number, i.e., they violate unitarity as discussed below. However, this absorption, which can be modeled using a complex scattering potential[19], is usually interpreted as the electrons undergoing inelastic scattering into lower energy states.

Models for pure dephasing or phase randomization have also been presented [26–28]. In these models, the various Feynman paths develop random phase factors as the particle traverses the device. Averaging over different realizations of the phase factors leads to an attenuation of the contributions of coherence to the observed transmission and reflection probabilities while still preserving unitarity. Statistical methods were shown to be consistent with experimentally observed Aharonov-Bohm oscillations in quantum rings [29]. However, it has been pointed out [30] that in the limit of complete incoherence, larger transmission probabilities in double-barrier structures are predicted using these phase randomization models than would have been predicted using Ohm's law; in contrast, Buttiker's dephasing probe model is consistent with Ohm's law in the limit of complete incoherence, which suggests that both complete phase and momentum randomization are required in the classical limit.

While the vast majority of research into dephasing of electron transport has focused on double barrier structures, less attention has been given to the problem of dephasing of spatial coherences on the transmission and reflection spectra above or within a single barrier and within the tunneling regime. In this work, different statistical models for the dephasing of spatial coherence for a one-dimensional rectangular barrier and using single particle Feynman paths are presented. The paper is organized as follows: after presenting the basic formulae for the transmission and reflection coefficients for transmission through a

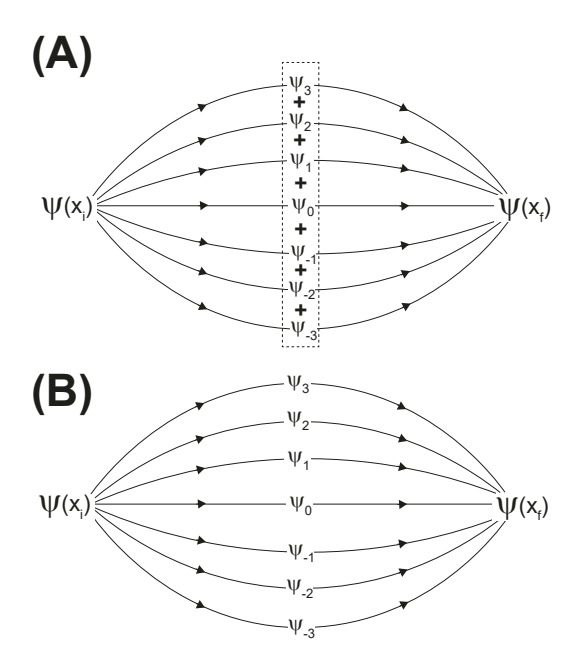


FIG. 1. Illustration of (A) coherent and (B) incoherent transport. (A) For coherent transport, the wave function at $x = x_f$, $\Psi(x_f)$, can be thought of as arising from a coherent superposition of all possible trajectories starting from the wave function at $x = x_i$, $\Psi(x_i)$, i.e., $\Psi(x_f) = \sum_n \Psi_n(x_f)$. (B) For fully incoherent transport, the coherence between all trajectories vanishes, and the various pathways add incoherently.

rectangular barrier of height V_0 in Section II, a Feynman pathway description of transmission and reflection above a rectangular barrier $(E > V_0)$ is presented in Section III. Three models of spatial dephasing that preserve unitarity are considered in Section IV. In Section V, it is demonstrated that in order to preserve unitarity in the tunneling regime $(E < V_0)$, a superposition of evanescent waves that represent the various Feynman paths for both transmitted and reflected wave functions cannot spatially dephase, i.e., $L_{\phi} \to \infty$ in the tunneling regime. Unlike for transmission above the barrier, however, wave absorption models for electrons within the barrier are shown to preserve unitarity. It should be noted that decoherence models where the environment changes state as a result of the scattering processes[31] are not considered in this work.

II. THE TRANSMISSION AND REFLECTION COEFFICIENTS FOR A 1D RECTANGULAR POTENTIAL BARRIER

First, we present the standard results for the transmission (T_0) and reflection (R_0) coefficients of a flux-normalized wave of energy E incident from the left to a 1D potential barrier of height V_0 and width L_B located between $x = L_0$ and $x = L_0 + L_B$. Experimentally, such a setup could be realized either in gated single tunnel junctions in either vertical or lateral quantum dots, or in quantum wires with an artificial barrier placed along the wire that acts as a barrier.

The wave function to the left of the barrier $(x < L_0)$ is given by:

$$\Psi(x) = \frac{e^{ikx}}{\sqrt{\frac{\hbar k}{m}}} + R_0 \frac{e^{-ikx}}{\sqrt{\frac{\hbar k}{m}}} \equiv \frac{e^{ikx}}{\sqrt{\frac{\hbar k}{m}}} + \Psi_R(x)$$
 (1)

where $\Psi_R(x)$ is the reflected wave function, and $k = \sqrt{\frac{2mE}{\hbar^2}}$ is the wave vector magnitude. The wave function to the right of the barrier $(x > L_0 + L_B)$ is given by:

$$\Psi(x) = T_0 \frac{e^{ikx}}{\sqrt{\frac{\hbar k}{m}}} \equiv \Psi_T(x) \tag{2}$$

where $\Psi_T(x)$ is the transmitted wave function.

The determination of R_0 and T_0 in Eqs.(1) and (2), which is a standard textbook problem in quantum mechanics[32], is typically accomplished by matching the wave function and its spatial derivative at $x = L_0$ and $x = L_0 + L_B$. For $E > V_0$, this procedure gives:

$$T_0 = \frac{e^{-ikL_B}}{\cos(k_1 L_B) - i\frac{k_1^2 + k^2}{2kk_1}\sin(k_1 L_B)}$$
(3)

$$R_0 = i \frac{\frac{k_1^2 - k^2}{2k_1 k} \sin(k_1 L_B) e^{2ikL_0}}{\cos(k_1 L_B) - i \frac{k_1^2 + k^2}{2k_1 k} \sin(k_1 L_B)} = i \frac{k_1^2 - k^2}{2k_1 k} \sin(k_1 L_B) e^{ik(2L_0 + L_B)} T_0$$
(4)

where $k_1 = \sqrt{\frac{2m(E-V_0)}{\hbar^2}}$ is the wave vector magnitude above the barrier.

In the tunneling regime, i.e., $E < V_0$, T_0 and R_0 are given by:

$$T_0 = \frac{e^{-ikL_B}}{\cosh(\kappa L_B) + i\frac{\kappa^2 - k^2}{2\kappa k_B}\sinh(\kappa L_B)}$$
(5)

$$R_0 = -i \frac{\frac{\kappa^2 + k^2}{2\kappa k} \sinh(\kappa L_B) e^{2ikL_0}}{\cosh(\kappa L_B) + i \frac{\kappa^2 - k^2}{2\kappa k} \sinh(\kappa L_B)} = -i \frac{\kappa^2 + k^2}{2\kappa k} \sinh(\kappa L_B) e^{ik(2L_0 + L_B)} T_0$$
 (6)

where $\kappa = \sqrt{\frac{2m(V_0 - E)}{\hbar^2}}$ is the magnitude of the complex wave vector within the barrier.

Given that the 1D flux operator is $\widehat{J}_X = \frac{\widehat{p}_X}{m} = -\frac{i\hbar}{m} \frac{\partial}{\partial x}$, conservation of flux requires that the sum of the magnitudes of the transmitted and reflected fluxes equals the total magnitude of the incident flux (which is taken to be unity due to flux-normalization):

$$\langle \Psi_T | \widehat{J}_X | \Psi_T \rangle - \langle \Psi_R | \widehat{J}_X | \Psi_R \rangle = \langle \Psi_T | \widehat{J}_X | \Psi_T \rangle + \left| \langle \Psi_R | \widehat{J}_X | \Psi_R \rangle \right| = 1 \tag{7}$$

Since $\langle \Psi_T | \widehat{J}_X | \Psi_T \rangle = |T_0|^2 \equiv \mathcal{T}$ represents the total transmission probability, and $-\langle \Psi_R | \widehat{J}_X | \Psi_R \rangle = |R_0|^2 \equiv \mathcal{R}$ represents the total reflection probability, the conservation of flux in Eq. (7) can be simply written as:

$$\mathcal{T} + \mathcal{R} = 1 \tag{8}$$

Eq. (8) is often referred to as the unitarity condition. For incident waves comprised of charge carriers such as electrons, Eq. (8) ensures that total charge (i.e., electron number) is conserved under the scattering process.

III. FEYNMAN PATHWAY DESCRIPTION OF TRANSMISSION ABOVE A RECTANGULAR POTENTIAL BARRIER

An alternative method to calculate the transmission and reflection coefficients for scattering from a rectangular potential barrier is to consider all Feynman pathways[14, 20–23] a quantum particle can follow due to scattering from the barrier. As illustrated in Fig. 2(A), $\Psi_T(x)$ can be written in terms of Feynman paths that are transmitted over the barrier (for $x > L_0 + L_B$):

$$\Psi_T(x) = \langle x | \Psi_T \rangle = \Psi_{T,0}(x) + \Psi_{T,2}(x) + \Psi_{T,4}(x) + \dots = \sum_{n=0}^{\infty} \Psi_{T,2n}(x)$$
 (9)

where $\Psi_{T,2n}(x)$, which represents a Feynman path corresponding to a transmitted wave that has undergone 2n bounces above the barrier, is given by:

$$\Psi_{T,2n}(x) = \langle x | \Psi_{T,2n} \rangle = |t_{k,k_1}|^2 e^{-ikL_B} e^{ik_1L_B} \left(|r_{k,k_1}|^2 e^{2ik_1L_B} \right)^n \frac{e^{ikx}}{\sqrt{\frac{\hbar k}{m}}} \equiv \tilde{t}_n \frac{e^{ikx}}{\sqrt{\frac{\hbar k}{m}}}$$
(10)

where $|\tilde{t}_n|$ is the transmission probability amplitude associated with the Feynman path $|\Psi_{T,2n}\rangle$, and $|t_{k,k_1}| = \frac{2\sqrt{kk_1}}{k+k_1}$, $|r_{k,k_1}| = \left|\frac{k-k_1}{k+k_1}\right|$ (see Appendix VIIA for more details). These

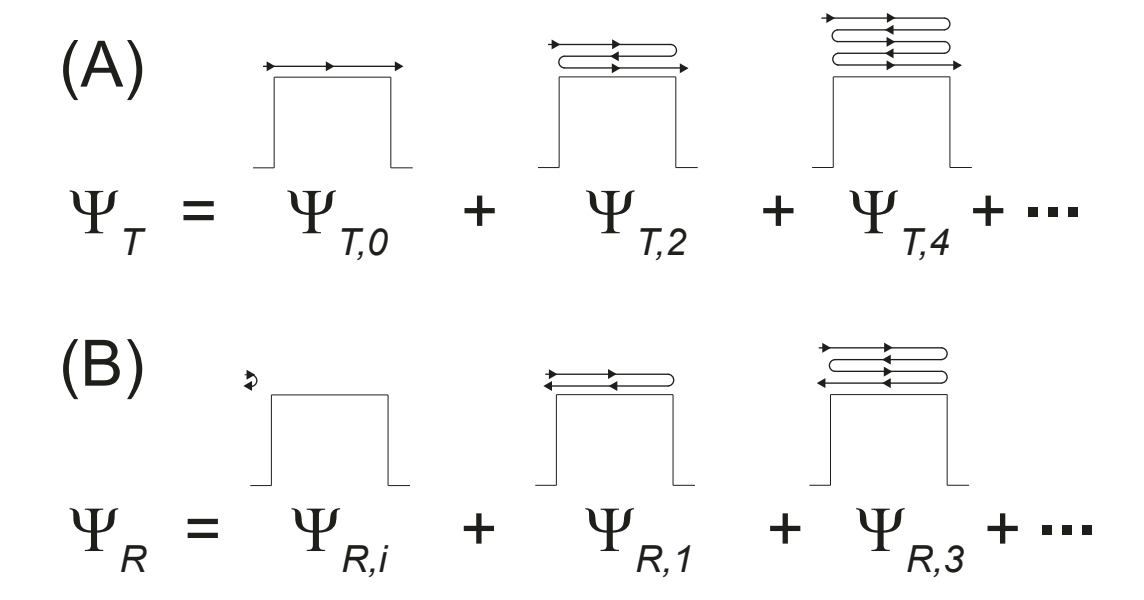


FIG. 2. Feynman paths for elastic scattering from a 1D potential barrier for $E > V_0$. (A) The transmitted wave function, Ψ_T [Eq. (9)], and (B) the reflected wave function, Ψ_R [Eq. (12)], can be interpreted as a coherent superposition of Feynman paths. In this case, the Feynman paths are analogous to light scattering found in Fabry-Perot scattering, where the barrier edges behave like semitransparent mirrors. All illustrated Feynman paths correspond to the same energy E (i.e., the vertical scale does not represent energy).

bouncing trajectories are analogous the scattering pathways found in Fabry-Perot etalons where the barrier edges act like leaky or semitransparent mirrors.

In Eq. (9), the Feynman paths can be explicitly summed to give:

$$\Psi_T(x) = \sum_{n=0}^{\infty} \tilde{t}_n \frac{e^{ikx}}{\sqrt{\frac{\hbar k}{m}}} = T_0 \frac{e^{ikx}}{\sqrt{\frac{\hbar k}{m}}}$$
(11)

where T_0 is given in Eq. (3).

Similarly, $\Psi_R(x)$ can be written as a sum of all Feynman paths corresponding to an incident wave being reflected from the barrier (for $x < L_0$):

$$\Psi_R(x) = \langle x | \Psi_R \rangle = \Psi_{R,i}(x) + \Psi_{R,1}(x) + \Psi_{R,3}(x) + \dots = \Psi_{R,i}(x) + \sum_{n=0}^{\infty} \Psi_{R,2n+1}(x)$$
 (12)

where $\Psi_{R,i}(x) = \langle x | \Psi_{R,i} \rangle = |r_{k,k_1}| e^{2ikL_0} \frac{e^{-ikx}}{\sqrt{\frac{\hbar k}{m}}}$ represents the Feynman path for a wave that is directly reflected from the potential barrier's left edge while $\Psi_{R,2n+1}(x)$, which represents

a Feynman path for a wave that has undergone 2n + 1 bounces above the barrier before ultimately being reflected, is given by:

$$\Psi_{R,2n+1}(x) = \langle x | \Psi_{R,2n+1} \rangle = -|t_{k,k_1}|^2 |r_{k,k_1}| e^{2ikL_0} e^{2ik_1L_B} \left(|r_{k,k_1}|^2 e^{2ik_1L_B} \right)^n \frac{e^{-ikx}}{\sqrt{\frac{\hbar k}{m}}} = \tilde{r}_n \frac{e^{-ikx}}{\sqrt{\frac{\hbar k}{m}}}$$
(13)

where $|\tilde{r}_n|$ is the reflection probability amplitude associated with the Feynman path $|\Psi_{R,2n+1}\rangle$.

The various Feynman paths in Eq. (12) can be explicitly summed to give:

$$\Psi_R(x) = |r_{k,k_1}|e^{2ikL_0} \left(1 - \frac{|t_{k,k_1}|^2 e^{2ik_1 L_B}}{1 - |r_{k,k_1}|^2 e^{2ik_1 L_B}}\right) \frac{e^{-ikx}}{\sqrt{\frac{\hbar k}{m}}} = R_0 \frac{e^{-ikx}}{\sqrt{\frac{\hbar k}{m}}}$$
(14)

where R_0 is given in Eq. (4).

From Eq. (9) and Eq. (14), both $|\Psi_T\rangle$ and $|\Psi_R\rangle$ can be interpreted as being a coherent superposition of all Feynman paths above the barrier. One consequence of $|\Psi_T\rangle$ and $|\Psi_R\rangle$ being a superposition of Feynman paths is that the total transmission and reflection probabilities will contain contributions from the interference between different Feynman paths. For example, the total transmission probability is given by:

$$\mathcal{T} = \langle \Psi_{T} | \widehat{J}_{X} | \Psi_{T} \rangle = \sum_{n=0}^{\infty} \langle \Psi_{T,2n} | \widehat{J}_{X} | \Psi_{T,2n} \rangle + \sum_{m < n} \langle \Psi_{T,2m} | \widehat{J}_{X} | \Psi_{T,2n} \rangle + \langle \Psi_{T,2n} | \widehat{J}_{X} | \Psi_{T,2n} \rangle$$

$$= \sum_{n=0}^{\infty} |\widetilde{t}_{n}|^{2} + \sum_{m < n} \left((\widetilde{t}_{m})^{*} \widetilde{t}_{n} + \widetilde{t}_{m} (\widetilde{t}_{n})^{*} \right) = \mathcal{T}_{\text{incoherent}} + \mathcal{T}_{\text{coherent}}$$
(15)

where

$$\mathcal{T}_{\text{coherent}} = |t_{k,k_1}|^4 \sum_{m < n} |r_{k,k_1}|^{2(n+m)} \left(e^{i2(n-m)k_1 L_B} + e^{-i2(n-m)k_1 L_B} \right)
= \frac{2|r_{k,k_1}|^2 \left(\cos\left(2k_1 L_B\right) - |r_{k,k_1}|^2 \right)}{1 + |r_{k,k_1}|^4 - 2|r_{k,k_1}|^2 \cos\left(2k_1 L_B\right)} \mathcal{T}_{\text{incoherent}}$$
(16)

is the contribution to \mathcal{T} due to the interference between different Feynman paths that make up $|\Psi_T\rangle$ in Eq. (9), and

$$\mathcal{T}_{\text{incoherent}} = |t_{k,k_1}|^4 \sum_{n=0}^{\infty} |r_{k,k_1}|^{4n} = \frac{|t_{k,k_1}|^4}{1 - |r_{k,k_1}|^4} = \frac{|t_{k,k_1}|^2}{1 + |r_{k,k_1}|^2}$$
(17)

is the incoherent contribution to the transmission probability.

Using Eq. (12), a similar calculation of the total reflection probability, \mathcal{R} , gives:

$$\mathcal{R} = -\langle \Psi_{R,i} | \widehat{J}_X | \Psi_{R,i} \rangle - \sum_{n=0}^{\infty} \langle \Psi_{R,2n+1} | \widehat{J}_X | \Psi_{R,2n+1} \rangle - \sum_{n=0}^{\infty} \langle \Psi_{R,i} | \widehat{J}_X | \Psi_{R,2n+1} \rangle + \langle \Psi_{R,2n+1} | \widehat{J}_X | \Psi_{R,i} \rangle$$

$$- \sum_{m < n} \langle \Psi_{R,2m+1} | \widehat{J}_X | \Psi_{R,2n+1} \rangle + \langle \Psi_{R,2n+1} | \widehat{J}_X | \Psi_{R,2m+1} \rangle$$
interference terms
$$= |r_{k,k_1}|^2 + \sum_{n=0}^{\infty} |\tilde{r}_n|^{2n} + \sum_{m < n} (\tilde{r}_m)^* \tilde{r}_n + \tilde{r}_m (\tilde{r}_n)^* + \sum_{n=0}^{\infty} r_{k,k_1} (\tilde{r}_n)^* + (r_{k,k_1})^* \tilde{r}_n$$

$$= \mathcal{R}_{\text{incoherent}} + \mathcal{R}_{\text{coherent}} \tag{18}$$

where

$$\mathcal{R}_{\text{coherent}} = -2|t_{k,k_1}|^2 \sum_{n=1} |r_{k,k_1}|^{2n} \cos(2nk_1L_B)
+ 2|t_{k,k_1}|^4 |r_{k,k_1}|^2 \sum_{m < n} |r_{k,k_1}|^{2(n+m)} \cos(2(n-m)(k_1L_B))
= -2|r_{k,k_1}|^2 \frac{\cos(2k_1L_B) - |r_{k,k_1}|^2}{1 + |r_{k,k_1}|^4 - 2|r_{k,k_1}|^2 \cos(2k_1L_B)} \mathcal{T}_{\text{incoherent}}
= -\mathcal{T}_{\text{coherent}}$$
(19)

is the contribution to \mathcal{R} due to the interference between different Feynman paths that make up $|\Psi_R\rangle$ in Eq. (12), and

$$\mathcal{R}_{\text{incoherent}} = |r_{k,k_1}|^2 + \sum_{n=0}^{\infty} |\tilde{r}_n|^{2n} = \frac{2|r_{k,k_1}|^2}{1 + |r_{k_1,k}|^2}$$
 (20)

is the incoherent contribution to \mathcal{R} .

As can be seen from Eq. (17), Eq. (16), Eq. (20), and Eq. (19), \mathcal{T} and \mathcal{R} satisfy the unitarity condition in Eq. (8):

$$\mathcal{T} + \mathcal{R} = \mathcal{T}_{\text{incoherent}} + \mathcal{R}_{\text{incoherent}} + \mathcal{T}_{\text{coherent}} + \mathcal{R}_{\text{coherent}}$$

$$= \mathcal{T}_{\text{incoherent}} + \mathcal{R}_{\text{incoherent}} = \frac{|t_{k,k_1}|^2 + 2|r_{k,k_1}|^2}{1 + |r_{k,k_1}|^2} = 1$$
(21)

IV. STATISTICAL MODEL OF DEPHASING USING FEYNMAN PATHWAYS

As discussed in the Introduction, statistical models have been used to estimate the effects of dephasing on the transmission probabilities in mesoscopic devices [26–28]. In the statistical

model of dephasing, phase factors are introduced between different electron pathways as a way to model the effects of scattering by impurities throughout the device. While in such models a single electron wave function is still fully phase-coherent, i.e., it can always be written as a linear superposition of pathways, averaging over different realization of electron wave functions results in an attenuation of the contribution of coherence to the transport properties in the device. Again, it should be noted that this contrasts with the Buttiker dephasing probe model in which the electron wave functions are truly decohered by effectively removing an electron and then putting it back into the device leading to both phase and momentum randomization.

In statistical dephasing models, the transmitted and reflected wave functions can be written as:

$$|\Psi_{T}\rangle = e^{i\phi_{0}^{T}}|\Psi_{T,0}\rangle + e^{i\phi_{2}^{T}}|\Psi_{T,2}\rangle + e^{i\phi_{4}^{T}}|\Psi_{T,4}\rangle + \dots = \sum_{n=0} e^{i\phi_{2n}^{T}}|\Psi_{T,2n}\rangle$$

$$|\Psi_{R}\rangle = e^{i\phi_{i}^{R}}|\Psi_{R,i}\rangle + e^{i\phi_{1}^{R}}|\Psi_{R,1}\rangle + e^{i\phi_{3}^{R}}|\Psi_{R,3}\rangle + \dots = e^{i\phi_{i}^{R}}|\Psi_{R,i}\rangle + \sum_{n=0} e^{i\phi_{2n+1}^{R}}|\Psi_{R,2n+1}\rangle$$
(22)

where $e^{i\phi_n^T}$ and $e^{\phi_m^R}$ are random phase factors for the n^{th} transmission [Eq. (9)] and m^{th} reflection [Eq. (12)] Feynman pathways above the barrier as illustrated in Fig. 2. Averaging the total transmission and reflection probabilities for different realization of electron wave functions in Eq. (22) gives the average transmission and reflection probabilities, $\langle \mathcal{T} \rangle$ and $\langle \mathcal{R} \rangle$, respectively:

$$\langle \mathcal{T} \rangle = \mathcal{T}_{\text{incoherent}} + \sum_{m < n} \tilde{t}_{m} \tilde{t}_{n}^{*} \left\langle e^{i(\phi_{2m}^{T} - \phi_{2n}^{T})} \right\rangle + \tilde{t}_{n} \tilde{t}_{m}^{*} \left\langle e^{i(\phi_{2n}^{T} - \phi_{2m}^{T})} \right\rangle$$

$$\langle \mathcal{R} \rangle = \mathcal{R}_{\text{incoherent}} + \sum_{n=0}^{\infty} \tilde{r}_{n} r_{k,k_{1}}^{*} \left\langle e^{i(\phi_{2n+1}^{R} - \phi_{i}^{R})} \right\rangle + \tilde{r}_{n}^{*} r_{k,k_{1}} \left\langle e^{-i(\phi_{2n+1}^{R} - \phi_{i}^{R})} \right\rangle$$

$$+ \sum_{m < n} \tilde{r}_{m} \tilde{r}_{n}^{*} \left\langle e^{i(\phi_{2m+1}^{R} - \phi_{2n+1}^{R})} \right\rangle + \tilde{r}_{n} \tilde{r}_{m}^{*} \left\langle e^{i(\phi_{2n+1}^{R} - \phi_{2m+1}^{R})} \right\rangle$$

$$(23)$$

Where $\langle \ldots \rangle$ denotes an average over the distribution of phases. For example,

$$\left\langle e^{i(\phi_{2n}^T - \phi_{2m}^T)} \right\rangle = \int d\phi_{2n}^T \int d\phi_{2m}^T g_{2n,2m}^T (\phi_{2n}^T, \phi_{2m}^T) e^{i(\phi_{2n}^T - \phi_{2m}^T)}$$
 (24)

where $g_{2n,2m}^T(\phi_{2n}^T,\phi_{2m}^T)$ is a joint probability distribution for the phases ϕ_{2n}^T and ϕ_{2m}^T .

In the following, three different ways in which the relative phases between Feynman paths are modeled are presented: **Model I**: uncorrelated phases, **Model II**: partially correlated phases, and **Model III**: correlated phases.

A. Model I: uncorrelated phases

If the phases in Eq. (22) between different Feynman paths are completely uncorrelated, i.e., $\langle \phi_{2n}^T \phi_{2m}^T \rangle = \langle \phi_{2n}^T \rangle \langle \phi_{2m}^T \rangle$ and $\langle \phi_{2n+1}^R \phi_{2m+1}^R \rangle = \langle \phi_{2n+1}^R \rangle \langle \phi_{2m+1}^R \rangle$ for all $n \neq m$, then the joint probability distributions are also completely uncorrelated, i.e., $g_{2n,2m}^T (\phi_{2n}^T, \phi_{2m}^T) = g_{2n}^T (\phi_{2n}^T) g_{2m}^T (\phi_{2m}^T)$ and $g_{2n+1,2m+1}^R (\phi_{2n+1}^R, \phi_{2m+1}^R) = g_{2n+1}^R (\phi_{2n+1}^R) g_{2m+1}^R (\phi_{2m+1}^R)$ for all n and m. It is further assumed that the phase distributions are identical for all Feynman paths since these trajectories occur over the same barrier [Fig. 2], i.e., $g_{2m+1}^R (\phi) = g_{2m}^T (\phi) = \overline{g}(\phi)$ for all m. We will also assume that the phases are normally distributed about $\phi = 0$, $\overline{g}(\phi) = \frac{1}{\sqrt{2\pi \frac{L_B}{L_\phi}}} e^{-\frac{\phi^2}{2\frac{L_B}{L_\phi}}}$. It has been pointed out[30] that the use of normally distributed phase distributions give essentially identical results to periodic phase distributions when $\frac{L_B}{L_\phi} < \frac{\pi^2}{32}$. For larger $\frac{L_B}{L_\phi}$, periodic phase distributions should be used. In this case, a periodic phase distribution was shown to given the same predicted conductance values for a Buttiker dephasing probe in a single channel [33]. Note that $\phi = 0$ corresponds to no extraneous phase factors due to scattering from impurities within the barrier. Using $\overline{g}(\phi)$, $\langle \phi \rangle = 0$ and $\langle \phi^2 \rangle = \frac{L_B}{L_\phi}$.

In this case, the average of product of phase factors in Eq. (23) is given by:

$$\left\langle e^{\pm i(\phi_n^{T(R)} - \phi_m^{T(R)})} \right\rangle = \left\langle e^{\pm i\phi_n^{T(R)}} \right\rangle \left\langle e^{\mp i\phi_m^{T(R)}} \right\rangle = e^{-\frac{L_B}{L_\phi}} \equiv \lambda_\phi$$
 (25)

Using Eq. (25), $\langle \mathcal{T} \rangle$ and $\langle \mathcal{R} \rangle$ in Eq. (23) become:

$$\langle \mathcal{T} \rangle = \mathcal{T}_{\text{incoherent}} + \lambda_{\phi} \sum_{m < n} \tilde{t}_{m} \tilde{t}_{n}^{*} + \tilde{t}_{n} \tilde{t}_{m}^{*}$$

$$= \mathcal{T}_{\text{incoherent}} + 2 \mathcal{T}_{\text{incoherent}} \lambda_{\phi} \sum_{n=1}^{\infty} |r_{k,k_{1}}|^{2n} \cos(2nk_{1}L_{B})$$

$$\langle \mathcal{R} \rangle = \mathcal{R}_{\text{incoherent}} + \lambda_{\phi} \sum_{n=0}^{\infty} \left(\tilde{r}_{n} r_{k,k_{1}}^{*} + \tilde{r}_{n}^{*} r_{k,k_{1}} \right) + \lambda_{\phi} \sum_{m < n} \left(\tilde{r}_{m} \tilde{r}_{n}^{*} + \tilde{r}_{n} \tilde{r}_{m}^{*} \right)$$

$$= \mathcal{R}_{\text{incoherent}} - 2 \mathcal{T}_{\text{incoherent}} \lambda_{\phi} \sum_{n=1}^{\infty} |r_{k,k_{1}}|^{2n} \cos(2nk_{1}L_{B})$$

$$(26)$$

where $\langle \mathcal{T} \rangle + \langle \mathcal{R} \rangle = 1$. In **Model I**, which has been previously considered[26], the contributions of the coherence terms to $\langle \mathcal{T} \rangle$ and $\langle \mathcal{R} \rangle$ in Eq. (26) are simply attenuated by a common factor of $\lambda_{\phi} < 1$.

B. Model II: partially correlated phase shifts

In **Model II**, it is assumed that that each traversal of the barrier is associated with a random phase. That is, taking $\phi_1^R = \phi_i^R + \phi_{1,f} + \phi_{1,b}$, where the subscripts "f" and "b" denote forward (left to right) and backward (right to left) paths above the barrier, $\phi_3^R = \phi_i^R + \phi_{1,f} + \phi_{1,b} + \phi_{2,f} + \phi_{2,b}$, and in general:

$$\phi_{2n+1}^R = \phi_i^R + \sum_{m=1}^{n+1} (\phi_{m,f} + \phi_{m,b}) = \phi_{n+1,f} + \phi_{n+1,b} + \phi_{2n-1}^R$$
(27)

Similarly, $\phi_0^T = \phi_i^R + \phi_{1,f}$, $\phi_2^T = \phi_i^R + \phi_{1,f} + \phi_{1,b} + \phi_{2,f}$, and in general:

$$\phi_{2n}^{T} = \phi_{i}^{R} + \phi_{n+1,f} + \sum_{m=1}^{n-1} (\phi_{m,f} + \phi_{m,b}) = \phi_{n+1,f} + \phi_{n,b} + \phi_{2n-2}^{T}$$
(28)

If all the various phases, $\phi_{j,f}$ and $\phi_{j,b}$, are normally distributed and uncorrelated with each other (i.e, $\langle \phi_n \phi_m \rangle = \langle \phi_n \rangle \langle \phi_m \rangle$ for $n \neq m$), then the average phase factors in Eq. (23) become:

$$\left\langle e^{i\left(\phi_{2n}^{T}-\phi_{2m}^{T}\right)}\right\rangle = \left\langle e^{i\left(\phi_{n+1,f}+\phi_{m+1,b}+\sum_{p=m+2}^{n}\left(\phi_{p,f}+\phi_{p,b}\right)\right)}\right\rangle$$

$$= \left\langle e^{i\phi_{n+1,f}}\right\rangle \left\langle e^{i\phi_{m+1,b}}\right\rangle \prod_{p=m+2}^{n} \left\langle e^{i\phi_{p,f}}\right\rangle \left\langle e^{i\phi_{p,b}}\right\rangle$$

$$= \left(\left\langle e^{i\phi}\right\rangle\right)^{2(n-m)} = e^{-(n-m)\frac{L_{B}}{L_{\phi}}} = (\lambda_{\phi})^{n-m}$$
(29)

As such, $\langle \mathcal{T} \rangle$ and $\langle \mathcal{R} \rangle$ in Eq. (23) become:

$$\langle \mathcal{T} \rangle = \mathcal{T}_{\text{incoherent}} \left(1 + 2 \sum_{n=1}^{\infty} |r_{k,k_1}|^{2n} \cos(2nk_1 L_B) (\lambda_{\phi})^n \right)$$

$$\langle \mathcal{R} \rangle = \mathcal{R}_{\text{incoherent}} - 2 \mathcal{T}_{\text{incoherent}} \sum_{n=1}^{\infty} |r_{k,k_1}|^{2n} \cos(2nk_1 L_B) (\lambda_{\phi})^n$$
(30)

in which case $\langle \mathcal{T} \rangle + \langle \mathcal{R} \rangle = 1$. This model is similar to the model developed by Pala et al.[27].

C. Model III: Completely correlated phases

As with **Model II**, the various Feynman paths still develop a phase factor over each round trip above the barrier. However, in **Model III**, the increment in phase factor is taken to be the same for each round trip above the barrier, which can be justified if the electron wave experiences the same scattering configuration for each round trip above the barrier. In this case, the phases are given by $\phi_{2n}^T = \phi_0 + 2n\phi$ and $\phi_{2n+1}^R = \phi_i^R + 2(n+1)\phi$. This results in an average phase factor of:

$$\left\langle e^{i\left(\phi_{2n}^{T} - \phi_{2m}^{T}\right)}\right\rangle = \left\langle e^{i2(n-m)\phi}\right\rangle = e^{-\frac{(n-m)^{2}L_{B}}{L_{\phi}}} = (\lambda_{\phi})^{(n-m)^{2}} \tag{31}$$

In this case, $\langle \mathcal{T} \rangle$ and $\langle \mathcal{R} \rangle$ in Eq. (23) are given by:

$$\langle \mathcal{T} \rangle = \mathcal{T}_{\text{incoherent}} + \frac{4kk_1}{k^2 + k_1^2} \sum_{n=1}^{\infty} \cos(2nk_1 L_B) \left(\frac{k - k_1}{k + k_1}\right)^{2n} (\lambda_{\phi})^{n^2}$$

$$\langle \mathcal{R} \rangle = \mathcal{R}_{\text{incoherent}} - \frac{4kk_1}{k^2 + k_1^2} \sum_{n=1}^{\infty} \cos(2nk_1 L_B) \left(\frac{k - k_1}{k + k_1}\right)^{2n} (\lambda_{\phi})^{n^2}$$
(32)

D. Comparison of Models I-III for transmission above a rectangular barrier

In Fig. 3, calculations of $\langle \mathcal{T} \rangle$ and $\langle \mathcal{R} \rangle$ for a rectangular barrier with $\sqrt{\frac{2mV_0}{\hbar^2}}L_B = 10$ in the presence of dephasing and evaluated using either **Model I** [red, Eq. (26)], **Model II** [yellow, Eq. (30)], or **Model III** [green, Eq. (32)] are shown for [Fig. 3(A)] $\frac{L_B}{L_{\phi}} = \frac{1}{4}$ and [Fig. 3(B)] $\frac{L_B}{L_{\phi}} = 1$.

Compared with the transmission spectrum for fully coherent transport [black, calculated using Eqs. (3) and (4)], \mathcal{T} at the resonance conditions $\frac{E}{V_0} = \frac{n^2 \hbar^2 \pi^2}{2m L_B^2 V_0}$ was smaller due to the attenuation of $\mathcal{T}_{coherent}$ in $\langle \mathcal{T} \rangle$. This difference became more noticeable as L_{ϕ} became smaller [Fig. 3(B) vs Fig. 3(A)]. For $\frac{E}{V_0} \gg 1$, all three models gave similar results. However, for $E \approx V_0$, noticeable differences between the three models were evident [Fig. 3, right]. These differences were due to the fact that for $E \approx V_0$, multiple Feynman paths contribute significantly to both $|\Psi_R\rangle$ and $|\Psi_T\rangle$, and thus $\mathcal{R}_{coherent}$ and $\mathcal{T}_{coherent}$ make up a larger fraction of $\langle \mathcal{R} \rangle$ and $\langle \mathcal{T} \rangle$, respectively. Attenuation of $\mathcal{T}_{coherent}$ for $E \approx V_0$ resulted in an increase of \mathcal{T} and a decrease of $\langle \mathcal{R} \rangle$ with increasing $\frac{E}{V_0}$.

Note that $\mathcal{T}_{\text{coherent}}$ involves a sum over interference terms between Feynman paths with path length differences ranging from $2L_B$ to ∞ . For $2k_1L_B \geq 2\pi$, the various $\cos(2nk_1L_B)$

terms in $\mathcal{T}_{\text{coherent}}$ add destructively except near the resonance condition $2k_1L_B \approx 2n\pi$ for integer n, in which case $\cos(2nk_1L_B) \approx 1$ and the terms add constructively leading to increased transmission. Since the interference terms in **Model III** are attenuated as $(\lambda_{\phi})^{n^2}$ compared with being attenuated by only λ_{ϕ} or $(\lambda_{\phi})^n$ for **Models I** and **II**, respectively, $\mathcal{T}_{\text{coherent}}$ for **Model III** will mainly be dominated by the interference of Feynman paths that don't appreciably differ in path length (i.e., small n). For example, $\mathcal{T}_{\text{coherent}}$ for **Model III** in Eq. (32) can be approximated under the condition that $\frac{L_B}{L_{\phi}} \gg 1$ by:

$$\mathcal{T}_{\text{coherent}} = \frac{4kk_1}{k^2 + k_1^2} \sum_{n=1}^{\infty} \left(\frac{k - k_1}{k + k_1}\right)^{2n} (\lambda_{\phi})^{n^2} \cos(2nk_1 L_B)$$

$$\approx \frac{4kk_1}{k^2 + k_1^2} \left(\frac{k - k_1}{k + k_1}\right) \lambda_{\phi} \cos(2k_1 L_B)$$
(33)

The origin of the negative differential resistance (NDR) observed at low $\frac{E}{V_0}$ for **Model III** in Fig. 3 is due to the fact that $\mathcal{T}_{\text{coherent}}$ in Eq. (33) is dominated by a single, oscillatory term when $\frac{L_B}{\lambda_{\phi}} \gg 1$. Note that an NDR was not observed for **Model I** since the sum in Eq. (26) was not truncated. However, there appeared to be a small NDR observed for **Model II** due to the fact that interference terms corresponding to larger path length differences were attenuated more relative to those corresponding to smaller path length differences, albeit to a lesser degree than in **Model III**. It should be further noted that an NDR was also observed in prior theoretical studies of the effects of electron-electron interactions on decoherence[34].

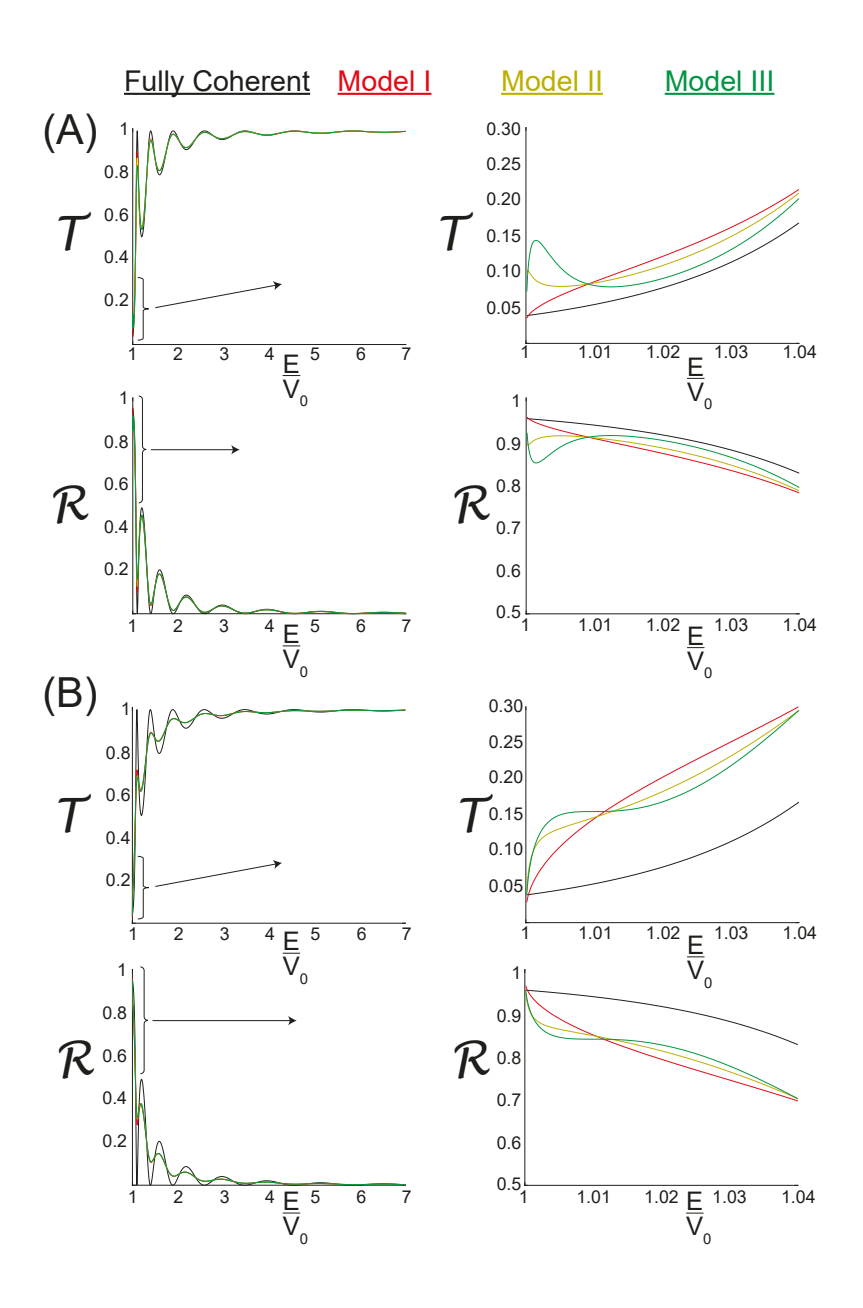


FIG. 3. Calculation of $\langle \mathcal{T} \rangle$ and $\langle \mathcal{R} \rangle$ in the presence of spatial decoherence using **Model I** [red, Eq. (26)], **Model II** [yellow, Eq. (30)], and **Model III** [green, Eq. (32)] as a function of $\frac{E}{V_0}$ with $\sqrt{\frac{2mV_0}{\hbar^2}}L_B = 10$. The fully coherent \mathcal{T} and \mathcal{R} are also shown for comparison [black curves calculated using Eqs. (3) and (4)]. In (A), $\frac{L_B}{L_\phi} = \frac{1}{4}$ was used. While all three models resulted in similar attenuation of the resonances in \mathcal{T} at $k_1L_B = n\pi$, the models exhibited very different behavior for $1 < \frac{E}{V_0} < 1.04$ due to differences in how the models attenuate interference contributions to $\langle \mathcal{T} \rangle$ and $\langle \mathcal{R} \rangle$. (B) Calculations using $\frac{L_B}{L_\phi} = 1$. Compared to (A), oscillations in \mathcal{T} were more attenuated as a result of increased spatial dephasing.

V. FEYNMAN PATHWAY DESCRIPTION IN THE TUNNELING REGIME

$$(A)$$

$$\Psi_{T} = \Psi_{T,0} + \Psi_{T,2} + \Psi_{T,4} + \cdots$$

$$(B)$$

$$\Psi_{R} = \Psi_{R,i} + \Psi_{R,1} + \Psi_{R,3} + \cdots$$

FIG. 4. Feynman paths for elastic scattering from a 1D potential barrier for $E < V_0$. (A) The transmitted wave function, Ψ_T [Eq. (34)], and (B) the reflected wave function, Ψ_R [Eq. (37)], can be interpreted as a coherent superposition of evanescent waves. In was the case in Fig. 2, the Feynman paths can be interpreted as evanescent analogues of Fabry-Perot scattering, where the barrier edges behave like semitransparent mirrors. All illustrated Feynman paths correspond to the same energy E (i.e., the vertical scale does not represent energy).

As illustrated in Fig. 4, the transmitted wave function for $E < V_0$ can still be written as a superposition of Feynman paths (for $x > L_0 + L_B$):

$$\Psi_T(x) = \Psi_{T,0}(x) + \Psi_{T,2}(x) + \dots = \sum_{n=0}^{\infty} \Psi_{T,2n}(x)$$
 (34)

where $\Psi_{T,2n}(x)$, which represents a Feynman path where an evanescent wave has undergone 2n bounces within the barrier before ultimately being transmitted, is given by:

$$\Psi_{T,2n}(x) = \langle x | \Psi_{T,2n} \rangle = i |t_{k,\kappa}|^2 e^{2i\phi_{k,\kappa}^T} e^{-ikL_B} e^{-\kappa L_B} \left(e^{2i\phi_{k,\kappa}^R} e^{-2\kappa L_B} \right)^n \frac{e^{ikx}}{\sqrt{\frac{\hbar k}{m}}} \equiv \tilde{t}_n \frac{e^{ikx}}{\sqrt{\frac{\hbar k}{m}}}$$
(35)

where
$$\kappa = \sqrt{\frac{2m(V_0 - E)}{\hbar^2}}$$
, $|t_{k,\kappa}| = \frac{2\sqrt{k\kappa}}{\sqrt{k^2 + \kappa^2}}$, $e^{i\phi_T^{k,\kappa}} = \frac{k - i\kappa}{\sqrt{k^2 + \kappa^2}}$, $e^{i\phi_R^{k,\kappa}} = \frac{k - i\kappa}{k + i\kappa}$ [see Appendix VII A].

Eq. (34) can be explicitly summed to give:

$$\Psi_T(x) = \sum_{n=0}^{\infty} \Psi_{T,2n}(x) = \sum_{n=0}^{\infty} \tilde{t}_n \frac{e^{ikx}}{\sqrt{\frac{\hbar k}{m}}} = T_0 \frac{e^{ikx}}{\sqrt{\frac{\hbar k}{m}}}$$
(36)

where T_0 is given in Eq. (5).

Similarly, the reflected wave function can still be written as a superposition of Feynman paths (for $x < L_0$)::

$$\Psi_R(x) = \Psi_{R,i}(x) + \Psi_{R,1}(x) + \Psi_{R,3}(x) + \dots = \Psi_{R,i} + \sum_{n=0}^{\infty} \Psi_{R,2n+1}(x)$$
 (37)

where $\Psi_{R,i}(x) = \langle x|\Psi_{R,i}\rangle = e^{i\phi_R^{k,\kappa}}e^{2ikL_0}\frac{e^{ikx}}{\sqrt{\frac{\hbar k}{m}}}$ again represents the initial reflected wave while $\Psi_{R,2n+1}(x)$, which represents a Feynman path where an evanescent wave has undergone 2n+1 bounces within the barrier before ultimately being reflected, is given by:

$$\Psi_{R,2n+1}(x) = \langle x | \Psi_{R,2n+1} \rangle = -i | t_{k,\kappa} |^2 e^{2i\phi_T^{k,\kappa}} e^{i\phi_R^{k,\kappa}} e^{2ikL_0} e^{-2\kappa L_B} \left(e^{2i\phi_R^{k,\kappa}} e^{-2\kappa L_B} \right)^n \frac{e^{-ikx}}{\sqrt{\frac{\hbar k}{m}}}$$

$$= \tilde{r}_n \frac{e^{-ikx}}{\sqrt{\frac{\hbar k}{m}}}$$
(38)

Eq. (37) can be be explicitly summed to give:

$$\Psi_{R}(x) = \left(e^{i\phi_{R}^{k,\kappa}}e^{2ikL_{0}} - i|t_{k,\kappa}|^{2}e^{2i\phi_{T}^{k,\kappa}}e^{i\phi_{R}^{k,\kappa}}e^{2ikL_{0}}e^{-2\kappa L_{B}}\left(e^{2i\phi_{R}^{k,\kappa}}e^{-2\kappa L_{B}}\right)^{n}\right)\frac{e^{-ikx}}{\sqrt{\frac{\hbar k}{m}}}$$

$$= R_{0}\frac{e^{-ikx}}{\sqrt{\frac{\hbar k}{m}}}$$
(39)

where R_0 is given in Eq. (6). From Eqs. (36) and (39), the transmitted and reflected waves can be interpreted as arising from all possible scattering paths within the barrier.

Performing calculations similar to those in Section III, the total transmission probability in the *absence* of dephasing is given by:

$$\mathcal{T} = \langle \Psi_T | \hat{J}_X | \Psi_T \rangle = \sum_{n=0}^{\infty} |\tilde{t}_n|^2 + \sum_{m < n}^{\text{interference of evanescent waves}} \tilde{t}_n \tilde{t}_m^* + \tilde{t}_m \tilde{t}_n^*$$

$$= \frac{8k^2 \kappa^2}{\sinh(2\kappa L_B)(k^2 + \kappa^2)^2} + \frac{8k^2 \kappa^2 \left((k + i\kappa)^4 + (k - i\kappa)^4 - 2(k^2 + \kappa^2)^2 e^{-2\kappa L_B} \right)}{\sinh(2\kappa L_B)(k^2 + \kappa^2)^2 \left(2(k^2 + \kappa^2)^2 \cosh(2\kappa L_B) - ((k + i\kappa)^4 + (k - i\kappa)^4) \right)}$$

$$\equiv \mathcal{T}_{\text{incoherent}} + \mathcal{T}_{\text{coherent}}$$

$$(40)$$

where

$$\mathcal{T}_{\text{incoherent}} = \frac{8k^2\kappa^2}{\sinh(2\kappa L_B)(k^2 + \kappa^2)^2} \tag{41}$$

Similarly, the total reflection probability is given by:

$$\mathcal{R} = -\langle \Psi_{R} | \widehat{J}_{X} | \Psi_{R} \rangle = |r_{k,\kappa}|^{2} + \sum_{n=0}^{\infty} |\widetilde{r}_{n}|^{2} + \sum_{n=0}^{\infty} |\widetilde{r}_{k,\kappa}\widetilde{r}_{n}^{*} + r_{k,\kappa}^{*}\widetilde{r}_{n} + \sum_{m< n} \widetilde{r}_{m}\widetilde{r}_{n}^{*} + \widetilde{r}_{n}\widetilde{r}_{m}^{*}$$

$$= 1 + \frac{8k^{2}\kappa^{2}e^{-2\kappa L_{B}}}{\sinh(2\kappa L_{B})(k^{2} + \kappa^{2})^{2}} - \frac{32k^{2}\kappa^{2}\cosh(\kappa L_{B})e^{-\kappa L_{B}}}{2(k^{2} + \kappa^{2})^{2}\cosh(2\kappa L_{B}) - ((k + i\kappa)^{4} + (k - i\kappa)^{4})}$$

$$= \frac{8k^{2}\kappa^{2}e^{-2\kappa L_{B}}}{\sinh(2\kappa L_{B})(k^{2} + \kappa^{2})^{2}(2(k^{2} + \kappa^{2})^{2}\cosh(2\kappa L_{B}) - (k + i\kappa)^{4} - (k - i\kappa)^{4})}$$

$$= \Re(k^{2}\kappa^{2}e^{-2\kappa L_{B}})$$

$$= \frac{8k^{2}\kappa^{2}e^{-2\kappa L_{B}}}{\sinh(2\kappa L_{B})(k^{2} + \kappa^{2})^{2}(2(k^{2} + \kappa^{2})^{2}\cosh(2\kappa L_{B}) - (k + i\kappa)^{4} - (k - i\kappa)^{4})}$$

$$= \Re(k^{2}\kappa^{2}e^{-2\kappa L_{B}})$$

$$= \Re(k^{2}\kappa^{2}e^{-2\kappa L_{B}})$$

$$= \frac{8k^{2}\kappa^{2}e^{-2\kappa L_{B}}}{\sinh(2\kappa L_{B})(k^{2} + \kappa^{2})^{2}(2(k^{2} + \kappa^{2})^{2}\cosh(2\kappa L_{B}) - (k + i\kappa)^{4} - (k - i\kappa)^{4})}$$

$$= \Re(k^{2}\kappa^{2}e^{-2\kappa L_{B}})$$

$$= \Re(k^{2}\kappa^{2}e^{-2\kappa L_{B}})$$

$$= \frac{8k^{2}\kappa^{2}e^{-2\kappa L_{B}}}{\sinh(2\kappa L_{B})(k^{2} + \kappa^{2})^{2}(2(k^{2} + \kappa^{2})^{2}\cosh(2\kappa L_{B}) - (k + i\kappa)^{4} - (k - i\kappa)^{4})}$$

$$= \Re(k^{2}\kappa^{2}e^{-2\kappa L_{B}})$$

$$= \frac{8k^{2}\kappa^{2}e^{-2\kappa L_{B}}}{\sinh(2\kappa L_{B})(k^{2} + \kappa^{2})^{2}}$$

$$= \frac{8k^{2}\kappa^{2}e^{$$

where

$$\mathcal{R}_{\text{incoherent}} = 1 + \frac{8k^2\kappa^2 e^{-2\kappa L_B}}{\sinh(2\kappa L_B)(k^2 + \kappa^2)^2}$$
(43)

From Eq. (40) and Eq. (42), $\mathcal{T} + \mathcal{R} = 1$.

We now wish to consider the affects of dephasing on \mathcal{T} and \mathcal{R} in the tunneling regime. For simplicity, consider the application of Model I. In this case, the interference terms in Eqs. (40) and (42) are attenuated by a factor of $e^{-\frac{L_B}{L_{\phi}}} = \lambda_{\phi} < 1$, which gives:

$$\langle \mathcal{T} \rangle = \mathcal{T}_{\text{incoherent}} + \lambda_{\phi} \frac{8k^{2}\kappa^{2} \left((k+i\kappa)^{4} + (k-i\kappa)^{4} - 2(k^{2}+\kappa^{2})^{2}e^{-2\kappa L_{B}} \right)}{\sinh(2\kappa L_{B})(k^{2}+\kappa^{2})^{2} \left(2(k^{2}+\kappa^{2})^{2}\cosh(2\kappa L_{B}) - ((k+i\kappa)^{4} + (k-i\kappa)^{4}) \right)}$$

$$\langle \mathcal{R} \rangle = \mathcal{R}_{\text{incoherent}} - \lambda_{\phi} \left(\frac{32k^{2}\kappa^{2}\cosh(\kappa L_{B})e^{-\kappa L_{B}}}{2(k^{2}+\kappa^{2})^{2}\cosh(2\kappa L_{B}) - ((k+i\kappa)^{4} + (k-i\kappa)^{4})} \right)$$

$$+ \lambda_{\phi} \left(\frac{8k^{2}\kappa^{2}e^{-2\kappa L_{B}} \left((k+i\kappa)^{4} + (k-i\kappa)^{4} - 2(k^{2}+\kappa^{2})^{2}e^{-2\kappa L_{B}} \right)}{\sinh(2\kappa L_{B})(k^{2}+\kappa^{2})^{2} \left(2(k^{2}+\kappa^{2})^{2}\cosh(2\kappa L_{B}) - (k+i\kappa)^{4} - (k-i\kappa)^{4} \right)} \right)$$

$$(44)$$

In Figure 5, the transmission and reflection spectra in the tunneling regime are shown for both the fully coherent case [Fig. 5(A) and calculated using Eqs. (5) and (6)] and for Model I [calculated using Eq. (44) for [Fig. 5(B)] $\frac{L_B}{L_{\phi}} = 1$ and for [Fig. 5(C)] $\frac{L_B}{L_{\phi}} = 5$]. Attenuating the contributions of the interference terms led to a violation of unitarity with $\langle \mathcal{T} \rangle + \langle \mathcal{R} \rangle > 1$ as seen in Fig. 5(B) and 5(C) [purple, dotted curves]. Violation of the unitarity condition

in Eq. (8) is due to the fact that [Eq. (43)] $\mathcal{R}_{incoherent}$ and [Eq. (41)] $\mathcal{T}_{incoherent}$ do not themselves satisfy the unitarity condition:

$$\mathcal{T}_{\text{incoherent}} + \mathcal{R}_{\text{incoherent}} = 1 + \frac{8k^2\kappa^2(1 + e^{-2\kappa L_B})}{\sinh(2\kappa L_B)(k^2 + \kappa^2)^2} > 1$$
(45)

As such, the condition that $\lambda_{\phi} \to 1$ (i.e., $L_{\phi} \to \infty$) in Eq. (44) for dephasing models must be satisfied in order to maintain unitarity in the tunneling regime.

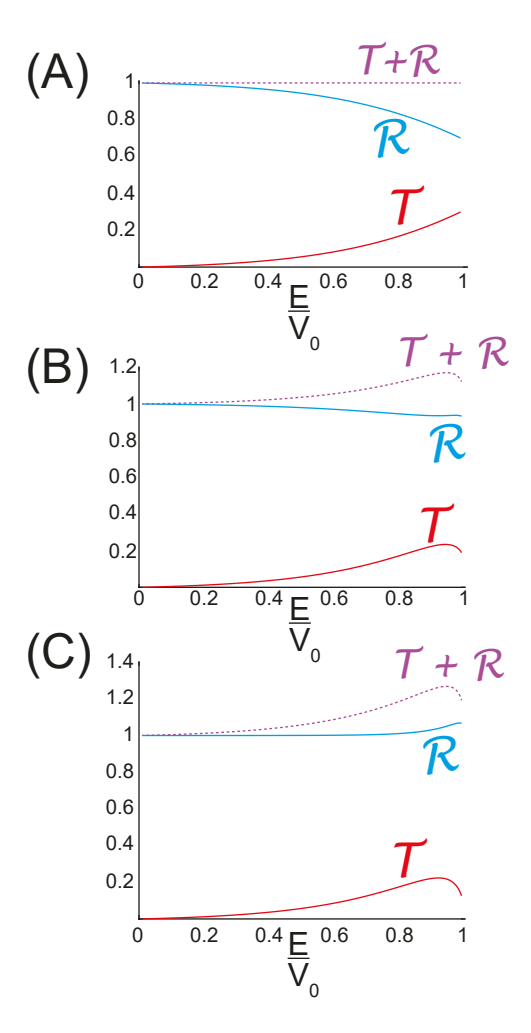


FIG. 5. Plots of (blue) $\langle \mathcal{R} \rangle$ and (red) $\langle \mathcal{T} \rangle$ vs $\frac{E}{V_0}$ in the tunneling regime for $\sqrt{\frac{2mV_0}{\hbar^2}}L_B=3$. (A) Fully coherent case, calculated using Eqs. (40) and (42), where unitarity is demonstrated from $\langle \mathcal{R} \rangle + \langle \mathcal{T} \rangle = 1$ (purple, dotted line). Plots of $\langle \mathcal{R} \rangle$ and $\langle \mathcal{T} \rangle$ calculated using Model **I** [Eq. (44)] for (B) $\frac{L_B}{L_\phi}=1$ and (C) $\frac{L_B}{L_\phi}=5$. Note that in both cases, the unitarity condition in Eq. (8) is violated since $\langle \mathcal{R} \rangle + \langle \mathcal{T} \rangle > 1$ (purple, dotted curve) in the presence of dephasing.

While the above arguments suggest that transport through a barrier must be fully phase coherent in order to preserve unitarity, this statement has meaning only if there are Feynman paths besides $\Psi_{T,0}$ and $\Psi_{R,i}$ that significantly contribute to $|\Psi_T\rangle$ [Eq. (34)] and $|\Psi_R\rangle$ [Eq. (37)], respectively. This requires:

$$\chi = \frac{|\tilde{t}_0|^2}{\mathcal{T}} = \left|1 - e^{2i\phi_R^{\kappa,k}} e^{-2\kappa L_B}\right|^2 < 1 \tag{46}$$

where χ represents the fraction of transmitted Feynman paths in $|\Psi_T\rangle$ corresponding to $|\Psi_{T,0}\rangle$. In Fig. 3, $\chi < 0.75$ for $\frac{E}{V_0} \geq 0.777$. Note in general, Eq. (46) will be satisfied as $E \to V_0$ meaning that as the energy of the incident wave approaches the barrier height, more Feynman paths other than $|\Psi_{T,0}\rangle$ and $|\Psi_{R,i}\rangle$ will significantly contribute to $|\Psi_T\rangle$ and $|\Psi_R\rangle$, respectively.

A. Partial absorption of evanescent waves preserves unitarity

While it was shown that dephasing of the coherence of evanescent waves within the barrier does not preserve unitarity, partial absorption of the evanescent waves within the barrier does. To see this, consider again $\Psi_T(x)$ in Eq. (34) and $\Psi_R(x)$ in Eq. (37). In the following, we will assume that the electron carriers can be "absorbed", i.e., inelastically scattered, as the electron travels through the barrier. In this case, the attenuation factor for going from the left to right barrier edge is given by $e^{-\alpha L_B}$ where we take $\alpha > 0$ in order that the evanescent wave is attenuated. In the wave absorption model, the attenuated $\Psi_R(x)$ and $\Psi_T(x)$ can be written as:

$$\Psi_{R}(x) = \Psi_{R,i}(x) + e^{-2\alpha L_{B}} \Psi_{R,1}(x) + e^{-4\alpha L_{B}} \Psi_{R,3}(x) + \dots = \Psi_{R,i}(x) + \sum_{n=1}^{\infty} e^{-2n\alpha L_{B}} \tilde{r}_{n} \frac{e^{-ikx}}{\sqrt{\frac{\hbar k}{m}}}$$

$$= \Psi_{R,i}(x) + \sum_{n=1}^{\infty} \tilde{\tilde{r}}_{n} \frac{e^{-ikx}}{\sqrt{\frac{\hbar k}{m}}}$$

$$\Psi_{T}(x) = e^{-\alpha L_{B}} \Psi_{t,0}(x) + e^{-3\alpha L_{B}} \Psi_{t,2}(x) + \dots = \sum_{n=0}^{\infty} \tilde{t}_{n} e^{-(2n+1)\alpha L_{B}} \frac{e^{ikx}}{\sqrt{\frac{\hbar k}{m}}}$$

$$= \sum_{n=0}^{\infty} \tilde{\tilde{t}}_{n} \frac{e^{ikx}}{\sqrt{\frac{\hbar k}{m}}}$$
(47)

where

$$\tilde{\tilde{r}}_n = e^{2n\alpha L_B} \tilde{r}_n = i|t_{k,\kappa}|^2 e^{2i\phi_T^{k,\kappa}} e^{i\phi_R^{k,\kappa}} e^{2ikL_0} e^{-2\kappa L_B\left(1+\frac{\alpha}{\kappa}\right)} \left(e^{2i\phi_R^{k,\kappa}} e^{-2\kappa L_B\left(1+\frac{\alpha}{\kappa}\right)}\right)^n$$

$$\equiv i|t_{k,\kappa}|^2 e^{2i\phi_T^{k,\kappa}} e^{i\phi_R^{k,\kappa}} e^{2ikL_0} e^{-2\kappa \tilde{L}_B} \left(e^{2i\phi_R^{k,\kappa}} e^{-2\kappa \tilde{L}_B} \right)^n$$

$$\tilde{\tilde{t}}_n = e^{-(2n+1)\alpha L_B} \tilde{t}_n = i|t_{k,\kappa}|^2 e^{2i\phi_{k,\kappa}^T} e^{-ikL_B} e^{-\kappa \tilde{L}_B} \left(e^{2i\phi_{k,\kappa}^R} e^{-2\kappa \tilde{L}_B} \right)^n$$

$$(48)$$

Thus, the effects of absorption/attenuation of the evanescent Feynman pathways within the barrier is just to increase the effective barrier length from L_B to $\tilde{L}_B = L_B \left(1 + \frac{\alpha}{\kappa}\right) > L_B$. As such, both \mathcal{T} and \mathcal{R} can be calculated from Eqs. (40) and (42), respectively, simply by replacing L_B with \tilde{L}_B . Thus the transmission spectrum in the tunneling regime should be identical to the case of fully phase-coherent tunneling in a barrier with an effective larger size of \tilde{L}_B . In this case, determining \tilde{L}_B and knowing L_B could be used to determine the effective absorption within the tunnel barrier (if any). It should be noted that while $\mathcal{T}+\mathcal{R}=1$ within the wave attenuation model for tunneling within a barrier, $\mathcal{T}+\mathcal{R}\neq 1$ for transmission above a barrier using the wave attenuation model.

VI. CONCLUSIONS

In this work, a Feynman pathway picture was used to describe the transmission and reflection probabilities for a 1D rectangular barrier in the presence of the dephasing of spatial coherences. For energies above the barrier, dephasing models that preserve unitarity require that the attenuation factors for the interference between any two Feynman paths are either identical (Model I) or depend only upon the difference in path lengths (Models II and III). In the tunneling regime, however, the evanescent waves cannot dephase within the barrier in order to preserve unitarity. While absorption models (without reinjection of electrons) for above barrier transmission violate unitarity, the evanescent waves in the tunneling regime can be absorbed within the barrier, which does satisfy unitarity. Wave absorption within the barrier results in transmission spectra that are equivalent to purely phase coherent tunneling in an effectively longer barrier. In this case, careful experimental studies of the transmission spectra in tunnel junctions, gated quantum wires, and other effective one-dimensional systems with a single barrier could be used to characterize the amount of absorption (if any) within the barrier for these materials. If materials in which the observed wave absorption is minimal inside the barrier are found, these materials can be doped with scatterers that act like " δ "-wells, in which case near unity phase-coherent tunneling through a single barrier can be generated. The theory using Feynman paths that was presented in this work could also be used to study transport in multibarrier systems (an application to double barrier systems and resonant tunneling is given in Supplementary Information). Though a single particle picture for the Feynman paths was used in this work, the theory can in principle be extended to Feynman paths representing multiple particles.

ACKNOWLEDGMENTS

We acknowledge support from the National Science Foundation under CHE - 1807724.

VII. APPENDIX

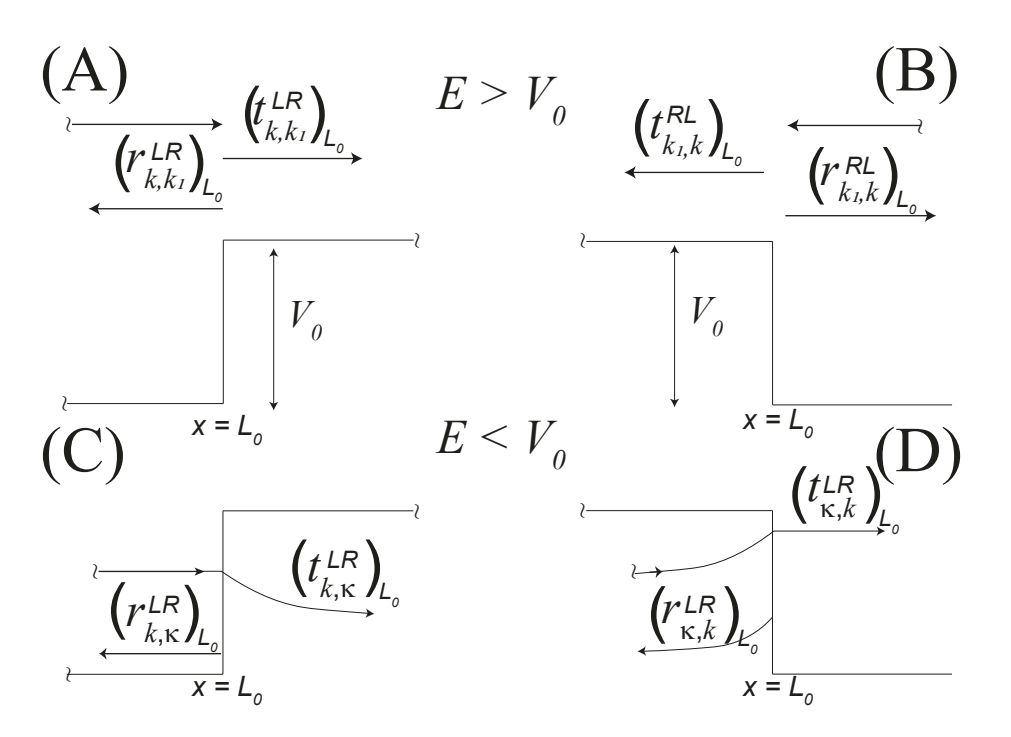


FIG. 6. Determination of scattering amplitudes from a step potential edge at $x=L_0$. For $E>V_0$, illustration of scattering processes to determine (A) $\left(t_{k,k_1}^{LR}\right)_{L_0}$ and $\left(r_{k,k_1}^{LR}\right)_{L_0}$, and (B) $\left(r_{k_1,k}^{RL}\right)_{L_0}$ and $\left(t_{k_1,k}^{RL}\right)_{L_0}$. For $E< V_0$, illustration of the scattering processes to determine (C) $\left(t_{k,\kappa}^{LR}\right)_{L_0}$ and $\left(r_{k,\kappa}^{LR}\right)_{L_0}$ along with (C) $\left(t_{\kappa,k}^{LR}\right)_{L_0}$ and $\left(r_{\kappa,k}^{LR}\right)_{L_0}$.

A. Determination of the reflection and transmission coefficients from a potential step of height V_0 for $E > V_0$

Consider again the case of a particle scattering from a potential step of height V_0 at $x = L_0$. For an incident wave from the left with $E = \frac{\hbar^2 k^2}{2m} > V_0$ as depicted in Fig. 6(A), the wave function for $x < L_0$ is given by:

$$\Psi(x) = \frac{e^{ikx}}{\sqrt{\frac{\hbar k}{m}}} + \left(r_{k,k_1}^{LR}\right)_{L_0} \frac{e^{-ikx}}{\sqrt{\frac{\hbar k}{m}}} \tag{49}$$

and for $x > L_0$

$$\Psi(x) = \left(t_{k,k_1}^{LR}\right)_{L_0} \frac{e^{ik_1 x}}{\sqrt{\frac{\hbar k_1}{m}}}$$
(50)

where $k_1 = \sqrt{\frac{2m}{\hbar^2}(E - V_0)}$, and $(t_{k,k_1}^{LR})_{L_0}$ and $(r_{k,k_1}^{LR})_{L_0}$ are the transmission and reflection coefficients from a potential step at $x = L_0$, respectively. Continuity of the wave function and its derivative at $x = L_0$ gives:

$$e^{ikL_0} + (r_{k,k_1}^{LR})_{L_0} e^{-ikL_0} = \sqrt{\frac{k}{k_1}} (t_{k,k_1}^{LR})_{L_0} e^{ik_1L_0}$$

$$\frac{k}{k_1} (e^{ikL_0} - (r_{k,k_1}^{LR})_{L_0} e^{-ikL_0}) = \sqrt{\frac{k}{k_1}} (t_{k,k_1}^{LR})_{L_0} e^{ik_1L_0}$$
(51)

from which

$$(r_{k,k_1}^{LR})_{L_0} = \frac{k - k_1}{k + k_1} e^{2ikL_0} \equiv r_{k,k_1} e^{2ikL_0}$$

$$(t_{k,k_1}^{LR})_{L_0} = \frac{2\sqrt{kk_1}}{k + k_1} e^{i(k-k_1)L_0} \equiv t_{k,k_1} e^{i(k-k_1)L_0}$$

$$(52)$$

For a wave incident from the right to a potential step at $x = L_0$ as depicted in Fig. 6(B), a similar calculation gives:

$$(r_{k_1,k}^{RL})_{L_0} = -r_{k,k_1} e^{-2ik_1 L_0}$$

$$(t_{k_1,k}^{RL})_{L_0} = t_{k,k_1} e^{i(k-k_0)L_0}$$

$$(53)$$

From the above equations, we have

$$\begin{vmatrix} \left(r_{k,k_1}^{LR} \right)_{L_0} \end{vmatrix} = \left| \left(r_{k_1,k}^{RL} \right)_{L_0} \right| \equiv |r_{k,k_1}|
\left| \left(t_{k,k_1}^{LR} \right)_{L_0} \right| = \left| \left(t_{k_1,k}^{RL} \right)_{L_0} \right| \equiv |t_{k,k_1}|$$
(54)

In all cases, the reflection and transmission coefficients satisfy the unitarity condition in Eq. (8):

$$\left| \left(t_{k,k_1}^{LR} \right)_{L_0} \right|^2 + \left| \left(r_{k,k_1}^{LR} \right)_{L_0} \right|^2 = \left| \left(t_{k_1,k}^{RL} \right)_{L_0} \right|^2 + \left| \left(r_{k_1,k}^{RL} \right)_{L_0} \right|^2 = |r_{k,k_1}|^2 + |t_{k,k_1}|^2 = 1 \tag{55}$$

These scattering coefficients were used in Sec. III.

B. Determination of reflection and transmission coefficients from a potential step of height V_0 for $E < V_0$

For a wave that is incident to a step potential at $x = L_0$ from the left with $E < V_0$ as illustrated in Fig. 6(C), the wave function for $x < L_0$ is given by:

$$\Psi(x) = \frac{e^{ikx}}{\sqrt{\frac{\hbar k}{m}}} + \left(r_{k,\kappa}^{LR}\right)_{L_0} \frac{e^{-ikx}}{\sqrt{\frac{\hbar k}{m}}}$$
(56)

where $\kappa = \sqrt{\frac{2m(V_0 - E)}{\hbar^2}}$, and $(r_{k,\kappa}^{LR})_{L_0}$ is the reflection coefficient for a step potential at $x = L_0$. The wave function for $x > L_0$ is given by:

$$\Psi(x) = \left(t_{k,\kappa}^{LR}\right)_{L_0} \frac{e^{-\kappa x}}{\sqrt{\frac{\hbar \kappa}{m}}} \tag{57}$$

where $(t_{k,\kappa}^{LR})_{L_0}$ is the transmission amplitude into the barrier.

Continuity of the wave function and its derivative at $x = L_0$ gives:

$$e^{ikL_0} + (r_{k,\kappa}^{LR})_{L_0} e^{-ikL_0} = \sqrt{\frac{k}{\kappa}} (t_{k,\kappa}^{LR})_{L_0} e^{-\kappa L_0}$$

$$\frac{ik}{\kappa} \left(e^{ikL_0} - (r_{k,\kappa}^{LR})_{L_0} \right) = -\sqrt{\frac{k}{\kappa}} (t_{k,\kappa}^{LR})_{L_0} e^{-\kappa L_0}$$
(58)

which gives

$$\begin{aligned}
\left(r_{k,\kappa}^{LR}\right)_{L_0} &= \frac{k - i\kappa}{k + i\kappa} e^{2ikL_0} \equiv e^{i\phi_R^{k,\kappa}} e^{2ikL_0} \\
\left(t_{k,\kappa}^{LR}\right)_{L_0} &= \frac{2\sqrt{k\kappa}}{k + i\kappa} e^{ikL_0} e^{\kappa L_0} \equiv |t_{k,\kappa}| e^{i\phi_T^{k,\kappa}} e^{ikL_0} e^{\kappa L_0}
\end{aligned} \tag{59}$$

where

$$|t_{k,\kappa}| = \frac{2\sqrt{k\kappa}}{\sqrt{k^2 + \kappa^2}}$$

$$e^{i\phi_T^{k,\kappa}} = \frac{k - i\kappa}{\sqrt{k^2 + \kappa^2}}$$

$$e^{i\phi_R^{k,\kappa}} = \frac{k - i\kappa}{k + i\kappa}$$
(60)

Note that $\left|\left(r_{k,\kappa}^{LR}\right)_{L_0}\right|^2=1$ since the transmitted wave in the barrier has imaginary flux.

Now consider a particle that exits a barrier step at $x = L_0$ from the left as illustrated in Fig. 6(D). In this case, the wave function for $x < L_0$ is given by:

$$\Psi(x) = \frac{e^{-\kappa x}}{\sqrt{\frac{\hbar \kappa}{m}}} + \left(r_{\kappa,k}^{LR}\right)_{L_0} \frac{e^{\kappa x}}{\sqrt{\frac{\hbar \kappa}{m}}} \tag{61}$$

and for $x > L_0$

$$\Psi(x) = \left(t_{\kappa,k}^{LR}\right)_{L_0} \frac{e^{ikx}}{\sqrt{\frac{\hbar k}{m}}} \tag{62}$$

where $k = \sqrt{\frac{2mE}{\hbar^2}}$.

Continuity of the wave function and its derivative at $x = L_0$ gives:

$$e^{-\kappa L_0} + (r_{\kappa,k}^{LR})_{L_0} e^{\kappa L_0} = \sqrt{\frac{\kappa}{k}} (t_{\kappa,k}^{LR})_{L_0} e^{ikL_0}$$

$$-\frac{\kappa}{ik} \left(e^{-\kappa L_0} - (r_{\kappa,k}^{LR})_{L_0} e^{\kappa L_0} \right) = \sqrt{\frac{\kappa}{k}} (t_{\kappa,k}^{LR})_{L_0} e^{ikL_0}$$
(63)

which gives

$$(t_{\kappa,k}^{LR})_{L_0} = i|t_{k,\kappa}|e^{i\phi_T^{k,\kappa}}e^{-ikL_0}e^{-\kappa L_0}$$

$$(r_{\kappa,k}^{LR})_{L_0} = -e^{i\phi_R^{k,\kappa}}e^{-2\kappa L_0}$$
(64)

For completeness, similar calculations of the transmission and reflection coefficients for the reverse processes depicted in Fig. 6(C) and 6(D) give:

$$\begin{split} \left(t_{k,\kappa}^{RL}\right)_{L_{0}} &= |t_{k,\kappa}| e^{i\phi_{T}^{k,\kappa}} e^{-ikL_{0}} e^{-\kappa L_{0}} \\ \left(r_{k,\kappa}^{RL}\right)_{L_{0}} &= e^{i\phi_{R}^{k,\kappa}} e^{-2ikL_{0}} \\ \left(t_{\kappa,k}^{RL}\right)_{L_{0}} &= i|t_{k,\kappa}| e^{i\phi_{T}^{k,\kappa}} e^{ikL_{0}} e^{\kappa L_{0}} \\ \left(r_{\kappa,k}^{RL}\right)_{L_{0}} &= -e^{i\phi_{R}^{k,\kappa}} e^{2\kappa L_{0}} \end{split} \tag{65}$$

These scattering coefficients were used in Section V.

[1] Y. Aharonov and D. Bohm. Significance of electromagnetic potentials in the quantum theory. *Phys. Rev.*, 115:485–491, 1959.

- [2] P. W. Anderson. Absence of diffusion in certain random lattices. *Phys. Rev.*, 109:1492–1505, 1958.
- [3] B. L. Altshuler, D. Kheml'nitzkii, A. I. Larkin, and P. A. Lee. Magnetoresistance and hall effect in a disordered two-dimensional electron gas. *Phys. Rev. B*, 22:5142, 1980.
- [4] M. F. Crommie, C. P. Lutz, and D. M. Eigler. Confinement of electrons to quantum corrals on a metal-surface. *Science*, 262:218–220, 1993.
- [5] E. J. Heller, M. F. Crommie, C. P. Lutz, and D. M. Eigler. Scattering and absorption of surface electron waves in quantum corrals. *Nature*, 369:464–466, 1994.
- [6] W. H. Zurek. Decoherence and the transition from quantum to classical. *Physics Today*, 44:36–44, 1991.
- [7] W. H. Zurek. Decoherence, einselection, and the quantum origins of the classical. *Rev. Mod. Phys.*, 75:715–775, 2003.
- [8] M. Buttiker. Role of quantum coherence in series resistors. Phys. Rev. B, 33:3021–3026, 1986.
- [9] M. J. McLennan, Y. Lee, and S. Datta. Voltage drop in mesoscopic systems: A numerical study using a quantum kinetic equation. *Phys. Rev. B*, 43:13846–13884, 1991.
- [10] S. Datta. Linear-response formulation of mesoscopic systems with arbitrary interactions. Phys. Rev. B, 46:9493–9500, 1992.
- [11] S. Hershfield. Equivalence of the multilead approach to dephasing and the self-consistent born approximation. *Phys. Rev. B*, 43:11586–11594, 1991.
- [12] S. Senozan, S. Turgut, and M. Tomak. A continuum model for dephasing in mesoscopic systems. *Physica E: Low-dimensional Systems and Nanostructures*, 43:1845–1852, 2011.
- [13] T. Stegmann, M. Zilly, O. Ujsaghy, and D.E. Wolf. Statistical model for the effects of phase and momentum randomization on electron transport. *Eur. Phys. J. B*, 85:264, 2012.
- [14] K.F. Freed. Path integrals and semiclassical tunneling, wavefunctions, and energies. *J. Chem. Phys.*, 56:692–697, 1972.
- [15] Y. Hu. An optical model of double-barrier resonant tunnelling oscillators. J. Phys. C: Solid State Phys., 21:L23–L29, 1988.
- [16] I-Hsing Tan, G. L. Snider, and E. L. Hu. Fabry-perot analysis of resonant tunneling structures. Superlattices and Microstructures, 10:67–72, 1991.
- [17] C. Benjamin and A. M. Jayannavar. A comparative study of some models of incoherence at the mesoscopic scale. *International Journal of Modern Physics B*, 17:4733–4748, 2003.

- [18] B. Ricco and M. Ya. Azbel. Physics of resonant tunneling. the one-dimensional double-barrier case. *Phys. Rev. B*, 29:1970–1981, 1984.
- [19] A. D. Stone and P. A. Lee. Effect of inelastic processes on resonant tunneling in one dimension. Phys. Rev. Lett., 54:1196–1199, 1985.
- [20] Y. Zohta. Scattering matrix theory of resonant tunneling. *Japanese J. Applied Physics*, 28:L2144–L2146, 1989.
- [21] Y. Zohta. Resonant tunneling time delay studied by feynman path integrals. *Solid State Communications*, 73:845–847, 1990.
- [22] Y. Zohta. Path-integral approach to resonant tunneling. Phys. Rev. B, 41:7879–7882, 1990.
- [23] Y. Zohta, K. Nakamura, and H. Ezawa. Difference in elastic scattering effects on resonant tunneling in one dimension and three dimensions. Solid State Communication, 80:885–889, 1991.
- [24] S. Datta. Electronic Transport in Mesoscopic Systems. Cambridge University Press, Cambridge, UK, 1997.
- [25] G. Hernandez. Fabry-perot with an absorbing etalon cavity. Applied Optics, 24:3062–3067, 1984.
- [26] J. H. Davies, J. C. Egues, and J. W. Wilkins. Effect of incoherence on current and shot noise in resonant tunneling: An exactly solvable model. *Phys. Rev. B*, 52:11259–11265, 1995.
- [27] M. G. Pala and G. Iannaccone. Statistical model of dephasing in mesoscopic devices introduced in the scattering matrix formalism. *Phys. Rev. B*, 69:235304, 2004.
- [28] M. G. Pala and G. Iannaccone. Effect of dephasing on the current statistics of mesoscopic devices. Phys. Rev. Lett., 93:256803, 2004.
- [29] A. E. Hansen, A. Kristensen, S. Pedersen, C. B. Sorensen, and P. E. Lindelof. Mesoscopic decoherence in aharonov-bohm rings. *Phys. Rev. B*, 64:045327, 2001.
- [30] S. Bandopadhyay, D. Chaudhuri, and A. M. Jayannavar. A comparative study of two phenomenological models of dephasing in series and parallel resistors. *Physics Letters A*, 374:813–818, 2010.
- [31] G. A. Fiete and E. J. Heller. Semiclassical theory of coherence and decoherence. Phys. Rev. A, 68, 2003.
- [32] R. L. Liboff. Introductory Quantum Mechanics. Addison Wesley, 2nd edition, 1991.
- [33] S. Pilgram, P. Samuelsson, H. Forster, and M. Buttiker. Full-counting statistics for voltage

- and dephasing probes. Phys. Rev. Lett., 97:066801, 2006.
- [34] R. Hartle, G. Cohen, D. R. Reichman, and A. J. Millis. Decoherence and lead-induced interdot coupling in nonequilibrium electron transport through interacting quantum dots: A hierarchical quantum master equation approach. *Phys. Rev. B*, 88:235426, 2013.